Emergence of unconventional spin glass-like state in κ-(ET)$_2$Cu[N(CN)$_2$]Cl by introducing weak randomness

Riku Yamamoto ,[1,*] Tetsuya Furukawa ,[1,2] Kazuya Miyagawa ,[3] Takahiko Sasaki ,[2] Kazushi Kanoda ,[3] and Tetsuaki Itou [1,†]

[1]*Department of Applied Physics, Tokyo University of Science, Tokyo 125-8585, Japan*
[2]*Institute for Materials Research, Tohoku University, Sendai 980-8577, Japan*
[3]*Department of Applied Physics, University of Tokyo, Tokyo 113-8656, Japan*

Recently, Urai *et al.* [Phys. Rev. Lett. **124**, 117204 (2020)] reported that an antiferromagnetic long-range-ordered state in κ-(ET)$_2$Cu[N(CN)$_2$]Cl changes into a quantum spin liquid via an unconventional spin glass-like state as randomness is introduced by x-ray irradiation. Here, we focused on the spin glass-like state and conducted a detailed investigation into it using ^{13}C-NMR measurements on 150-h x-ray-irradiated κ-(ET)$_2$Cu[N(CN)$_2$]Cl. We found that the spin glass-like state is composed of two components: the major component inherits the spin structure of nonirradiated κ-(ET)$_2$Cu[N(CN)$_2$]Cl, whereas the minor component differs from that of nonirradiated κ-(ET)$_2$Cu[N(CN)$_2$]Cl. We also found that in the spin glass-like state, spin moments fluctuate very slowly around stable directions even at low temperatures, which is very likely related to the Griffiths physics.

I. INTRODUCTION

The impact of randomness (quenched disorder) on materials is a long-standing issue in condensed matter physics. Randomness effects on antiferromagnetic (AFM) long-range-ordered (LRO) states have been actively studied both experimentally and theoretically [1–5]. Experimentally, various materials exhibiting AFM LRO states (two-dimensional (2D) Heisenberg antiferromagnets [6], spinel oxides [7,8], cuprates [9–11], and Zn paratacamites [12–14]) have been studied, and it has been reported that the AFM LRO states in these systems are destroyed by strong randomness. Theoretical studies have shown that randomness is as important as frustration in the stabilization of a quantum disordered state [quantum spin liquid (QSL)] [15–17].

Recently, an x-ray-irradiated organic weak Mott insulator, κ-(ET)$_2$Cu[N(CN)$_2$]Cl (where ET is bis(ethylenedithio) tetrathiafulvalene, hereafter abbreviated as κCl), has been studied, and it has been reported that the AFM LRO state realized in this system turns into a QSL-like state through a spin glass (SG)-like state upon increasing irradiation time [18]. It is surprising that even though x-ray irradiation causes only weak randomness in this organic material [18], it causes a large change in magnetic state. This cannot be explained by the conventional framework of the randomness effect on pure spin systems and probably requires Mottness-related discussion beyond the framework of random magnetism, e.g., a relationship to the electronic Griffiths phase [19,20], which is

thought to appear in the charge sector near the Mott transition [21].

A recent study [22] reported that x-ray irradiation to the quasi-two-dimensional organic family κ-(ET)$_2$X (where X is a monovalent anion) induces molecular defects in the insulating anion layers, which moderately disturbs the periodic potential in the conducting ET layers. This x-ray irradiation makes it possible to conduct systematic studies of a system with controlled randomness in an identical material because the amount of randomness increases with increasing irradiation time. The weak Mott insulator κCl, which exhibits an AFM LRO state with the transition temperature $T_N = 23$ K [23,24], was used to study the change of the AFM LRO state with randomness (x-ray irradiation). The studies in [21,25] showed that 500-h irradiation drives the AFM LRO state into a QSL-like state. Note that the amount of randomness is expected to be almost saturated in κCl after 500 h [22].

The key question, "How does the AFM LRO state turn into the QSL state?," has been answered very recently by Urai *et al.*'s systematic study [18]. The AFM LRO state collapses into the QSL state via an unusual SG-like state. The surprising point is that the collapse of the AFM order occurs even under a sparse distribution of disorder centers with $l = 200$–700 Å, which is probably attributable to κCl being located near the Mott transition. They claimed that the features of the SG-like state are as follows: (i) the magnitude of frozen moments is reduced and distributed, (ii) the moments do not inherit the spin structure of the AFM moments in the nonirradiated κCl but are randomly oriented, (iii) a QSL-like component exists in some parts of the system, (iv) paramagnetic-like spins exist in some parts of the system, and (v) the inhomogeneity of the system increases at low temperatures. Features (i)–(iii) were speculated from ^{1}H-NMR spectra and features (iv) and (v) from the behavior of the ^{1}H-NMR spin-lattice relaxation rate.

―――――――
*Present address: Los Alamos National Laboratory, Los Alamos, New Mexico, USA; riku.yamamoto@lanl.gov
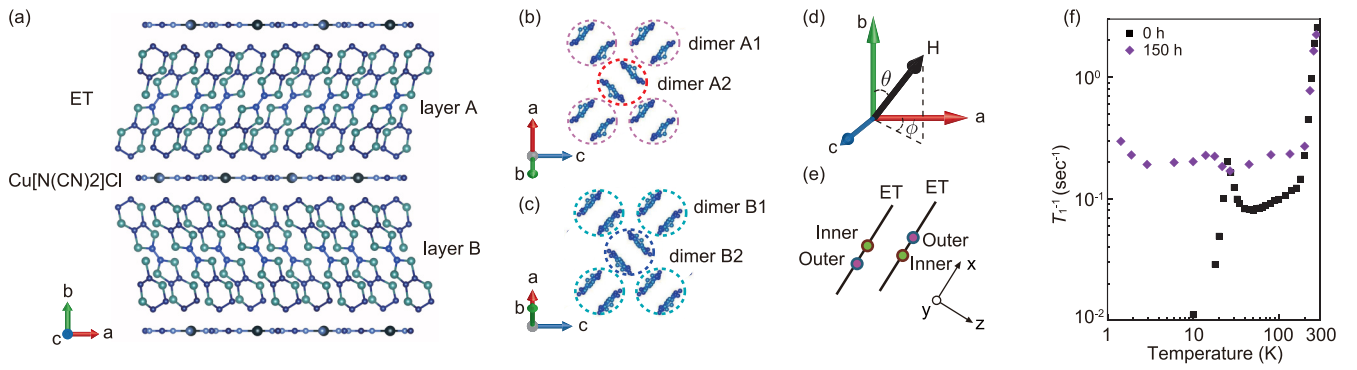†tetsuaki.itou@rs.tus.ac.jp

FIG. 1. Properties of κCl. (a) The layered structure of κCl (*Pnma* space group). The conducting ET layers are stacked alternately with the nonmagnetic insulating anion Cu[N(CN)$_2$]Cl layers. The defects induced by x-ray irradiation are in the anion layers [27] (local rearrangements of the C-N bonds in the anion [28,29]). The ET layers are divided into A and B layers. (b, c) In-plane arrangements of the ET molecules in layers A and B in κCl. Each layer includes two dimers (A1, A2, B1, and B2). These notations are after Ref. [30]. The A layer and B layer are related by a mirror operation. The dimers A1 and A2, and B1 and B2, are related by a glide operation. (d) Crystallographic axes and our definition of the angles (θ, ϕ). H denotes the direction of the magnetic field. (e) ^{13}C nuclei (the closed circles) at the inner and outer sites with different hyperfine fields in the dimer of ET molecules. (f) The spin-lattice relaxation rate T_1^{-1} of ^{1}H nuclei for the present ^{13}C-enriched 0h-κCl and 150h-κCl samples. The data of the 0h-κCl sample are from the previous study [23].

These suggestions do not give a conclusive answer to the question. Although ^{1}H-NMR for κCl can provide information on the presence or absence of frozen moments, it cannot provide detailed information on the spin state. This is because ^{1}H nuclei, which are at the terminal of the molecule, have a small hyperfine coupling because the density of the highest occupied molecular orbital in ET is concentrated in the center of the molecule [26]. Indeed, ^{1}H spectra are difficult to discuss small shifts, which are usually masked by spectral broadening due to the large ^{1}H nuclear-nuclear magnetic-dipole coupling. More importantly, the large ^{1}H nuclear-nuclear coupling makes it impossible to obtain the intrinsic (electronic origin) spin-spin relaxation rate T_2^{-1} of ^{1}H-NMR, which can illuminate the possibly important factor of slow dynamics for an SG state. To provide a more detailed discussion for the unconventional SG-like state and reinforce the discussions of the work in [21], we carried out ^{13}C-NMR measurements for a ^{13}C-enriched κCl single crystal irradiated with x rays for 150 h. Because of the large hyperfine coupling of ^{13}C nuclei, we can discuss the detailed information on the SG-like state from the ^{13}C-NMR spectra, T_1^{-1}, and T_2^{-1}.

II. EXPERIMENT

We prepared a single crystal of κCl [Figs. 1(a)–(c)], which was grown using the conventional electrochemical method, in which ^{13}C was enriched for the doubly bonded carbon sites at the center of ET. The dimensions of the measured crystal were approximately 0.96 mm $\times$ 1.5 mm $\times$ 0.23 mm (thickness). This is the same crystal that was used to obtain ^{13}C-NMR data without x-ray irradiation in the previous paper [21]. To discuss the effect of weak x-ray irradiation, we irradiated this crystal with white x rays at room temperature using a nonfiltered tungsten target at 40 kV and 20 mA after the measurements for the nonirradiated sample had been completed. The dose rate was approximately 0.5 MGy/h. To attain a uniform dose over the sample, (i) we used a sample

sufficiently thinner than the x-ray attenuation length, $\sim$1 mm, which was calculated for the present compound [31], and (ii) we irradiated both sides of the sample. The total irradiation time for this sample was 150 h. There is another factor that affects the magnitude of randomness. The terminal ethylene groups of the ET molecule fluctuate between two conformations at high temperatures and freeze around 70 K. When the cooling rate around 70 K is typically faster than 1 K/min, the terminal ethylene groups freeze randomly below 70 K [32,33]. This molecular freezing causes a quenched disordered effect for the electronic state. To eliminate this quenched disordered effect, we set the cooling rate at 0.1 K/min around 70 K.

We performed ^{13}C-NMR measurements for the 150-h-irradiated κCl (150h-κCl) sample under a magnetic field of 8.0 T. For comparison, we also showed previously obtained ^{13}C-NMR data under 8.0 T before x-ray irradiation (0h-κCl), which was reported in the previous work [21]. The directions of the magnetic fields are almost perpendicular to the conducting layers (ac plane), and the angles (θ, ϕ) between the external field and the crystal axes [Fig. 1(d)] ($\theta \sim 8.5°$, $\phi \sim 6°$) for 0h-κCl and ($\theta \sim 6.0°$, $\phi \sim 60°$) for 150h-κCl, which were determined by analyzing the NMR spectral lines and oscillations of the spin-spin relaxation curves at high temperatures. The NMR spectra, which come from the two neighboring ^{13}C sites (inner and outer sites) with different hyperfine tensors in an ET molecule [Fig. 1(e)], were obtained by Fourier-transforming the spin-echo signals following a ($\pi/2$)-τ-π pulse sequence. The widths of the $\pi/2$ and π pulses were typically 3 and 6 μs, respectively, and thus, the frequency range in which the NMR spectra can be observed precisely is approximately $f_0 \pm 50$ kHz, where f_0 is the center frequency. The observed NMR spectra of 150h-κCl (0h-κCl) are broadened (shifted) beyond this range at low temperatures. We measured spin-echo signals at varying center frequencies with 50-kHz intervals, and the entire spectra were then constructed by combining these individual spectra. The spin-lattice relaxation rate T_1^{-1} was obtained from
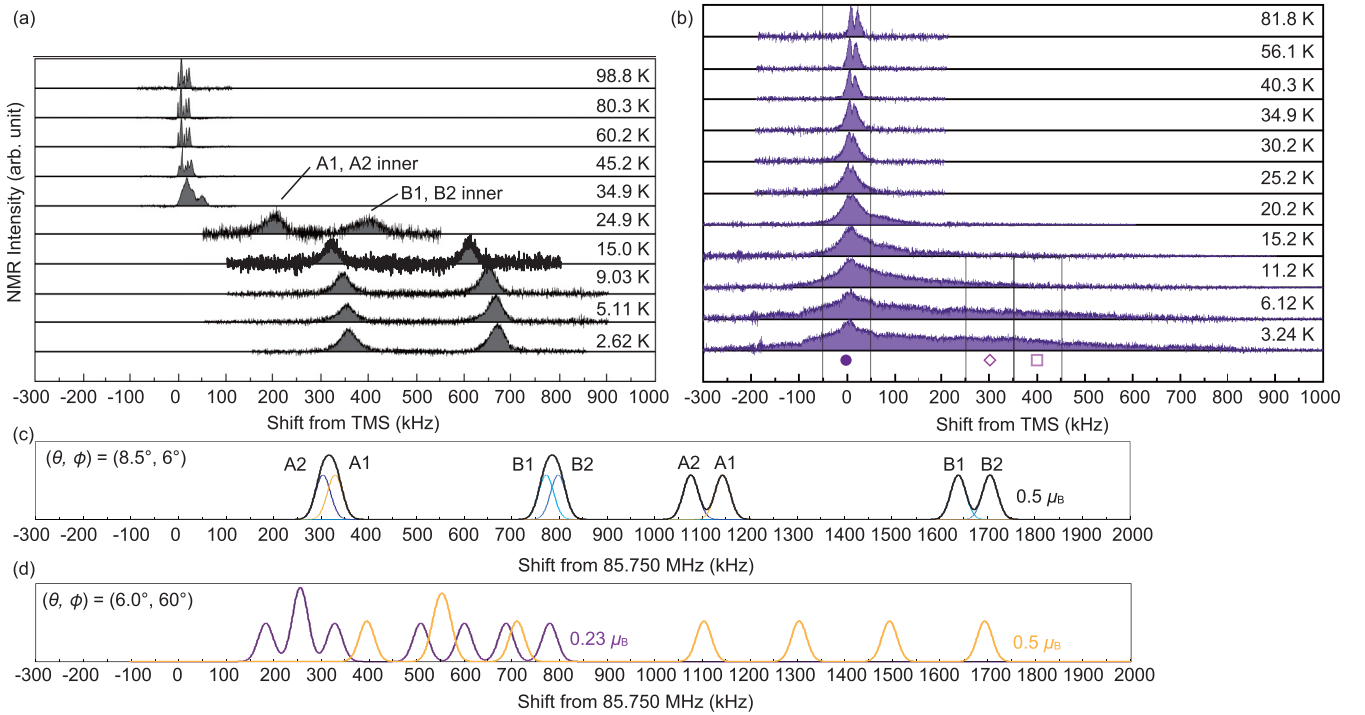
FIG. 2. ^{13}C-NMR spectra. The spectra of (a) 0h-κCl and (b) 150h-κCl. The shifts are relative to tetramethylsilane (TMS). The lines and symbols indicate the analyzed frequency ranges and the relaxation rates in them, 0 ± 50 kHz (solid dark purple circles), 300 ± 50 kHz (open purple diamonds), and 400 ± 50 kHz (open light purple squares). These symbols are used in Figs. 3 and 4. The spectra of 0h-κCl are from the previous study [21]. The simulated spectra of 0h-κCl in the AFM ordered phase, using the shift tensor [37], (c) the angles ($\theta \sim 8.5°$, $\phi \sim 6°$), and the magnitude of the ordered magnetic moments ($0.5\mu_B$ [23,30]), and (d) the angles ($\theta \sim 6.0°$, $\phi \sim 60°$), and the magnitude of the ordered magnetic moments ($0.5\mu_B$ and $0.23\mu_B$). The direction of the moment is assumed to be completely directed toward the c axis in this simulation.

the recovery of the frequency-integrated Fourier-transformed spin-echo intensity after the saturation comb pulses. We fitted the recovery curves of nuclear magnetization $M(t)$ using the stretched-exponential function

$$1 - M(t)/M(\infty) = A \exp\left\{-\left(\frac{t}{T_1}\right)^\beta\right\}, \qquad (1)$$

where A is a fitting parameter, t is the interval time between the last saturation comb pulse and the $\pi/2$ pulse, and β is the stretching exponent.

The spin-spin relaxation rate (the spin-echo decay rate) T_2^{-1} was obtained from the decay of the spin-echo intensity. We fitted spin-echo intensity curves $M(2\tau)$ to the following relation to obtain T_2 for both samples at high temperatures:

$$M(2\tau) = B\left\{\sum_{i=1}^{4} \cos\left(2\pi\frac{J_i}{2}2\tau\right) + C\right\} \exp\left\{-\left(\frac{2\tau}{T_2}\right)^2\right\}, \qquad (2)$$

where C and B are fitting parameters and J_i (in kilohertz) is the Pake-doublet coupling and fixed at values {($J_1 \sim 1.2$, $J_2 \sim 1.2$, $J_3 \sim 1.6$, $J_4 \sim 1.6$) for 150h-κCl and ($J_1 \sim 0.75$, $J_2 \sim 0.75$, $J_3 \sim 2.0$, $J_4 \sim 2.0$) for 0h-κCl}, which were expected for the above-mentioned (θ, ϕ) values (for details, see the Supplemental Material of the previous paper [21]). At high temperatures, the rates T_1^{-1} and T_2^{-1} of both 0h-κCl and 150h-κCl were obtained from the integrated intensity of the entire

spectra. On the other hand, at low temperatures where the ^{13}C-NMR spectra show huge shifts or broadening, the rates were obtained from the integrated intensity over a limited frequency range. The rates of 0h-κCl below T_N ($\sim$30 K under 8 T [34,35]) were obtained from the integrated intensity only of the inner ^{13}C-site spectra, and the rates of 150h-κCl at low temperatures are analyzed in the three different frequency ranges, namely, 0 ± 50, 300 ± 50, and 400 ± 50 kHz, which are shown in Fig. 2(b). In this situation, we obtained T_1 from Eq. (1), and T_2 was obtained from the following relation because the Pake-doublet oscillations were no longer realized under the experimental condition:

$$M(2\tau) = B\exp\left\{-\left(\frac{2\tau}{T_2}\right)^2\right\}. \qquad (3)$$

The details of the T_2 analysis were explained in the Supplemental Material of the previous paper [21].

In addition to the main ^{13}C-NMR measurements, we performed ^{1}H-NMR measurements for the ^{13}C-enriched 150h-κCl sample under 3.7 T to compare the effect of the present 150-h x-ray irradiation with the effect reported in the previous ^{1}H-NMR work. We found that with decreasing temperature, ^{1}H-NMR T_1^{-1} of the 150h-κCl sample begins to increase at 20 K, and peaks at around 10 K, but turns up below 3 K [Fig. 1(f)]. This ^{1}H-NMR T_1^{-1} behavior is similar to that of the 120-h-irradiated κCl sample in the previous work [18]. This result suggests that the present ^{13}C-enriched

150h-κCl sample has as much x-ray-irradiation effect as the 120-h-irradiated sample in the previous work [18].

III. RESULTS AND DISCUSSION

A. ^{13}C-NMR spectra

Figure 2 shows the temperature dependence of the ^{13}C-NMR spectra of 0h-κCl [Fig. 2(a)] and 150h-κCl [Fig. 2(b)]. The space group of κCl is *Pnma*, and the unit cell contains four ET dimers [A1, A2, B1, and B2; Figs. 1(b) and 1(c)], which are equivalent under zero magnetic field (or in the case that the applied magnetic field is exactly parallel to the *a*, *b*, or *c* axis). In each ET dimer, the ^{13}C sites are composed of two inequivalent sites, namely, the inner and outer sites [Fig. 1(e)]. Thus, in the case that an external magnetic field is applied along an arbitrary direction except the highly symmetric directions, there are eight (4×2) inequivalent magnetic ^{13}C sites. This effect and the Pake-doublet effect cause 16 NMR lines in total. Consequently, the NMR spectra of κCl at high temperatures become complex, giving information on (θ, ϕ), which is slightly deviated from ($0°$, $0°$), as explained in the previous section.

Below T_N, the spectra of 0h-κCl show two clear peaks, which have large shifts to positive frequencies due to the AFM LRO moments. When an external magnetic field was applied exactly along the *b* axis, the A1, A2, B1, and B2 dimers would become equivalent in the paramagnetic phase. Even under the AFM phase, A1, A2, B1, and B2 would also become equivalent when the amplitude of the magnetic field along the *b* axis is larger than that of the spin-flop field ($\sim$0.3 T) [36]. In this case, the AFM moments are almost directed toward the *c* axis owing to the competition of the Zeeman effect and the Dzyaloshinskii-Moriya interaction [30], and the inner and outer sites each show a single peak with positive frequency shifts (all hyperfine fields become positive in this case). In reality, however, we observed not a single peak but two peaks for the inner site spectra. This is because the direction of the applied magnetic field slightly deviated from the *b* axis. To perform peak assignment, we performed a spectral simulation of the AFM LRO state. In this spectral simulation, we used the angles ($\theta \sim 8.5°$, $\phi \sim 6°$) and the magnitude of the moments of $0.5\mu_B$ [23,30]. The direction of the moments is assumed to be directed toward the *c* axis completely. From this simulated spectrum [Fig. 2(c)], we found that the left peak consists of the inner sites of A1 and A2 and the right peak consists of those of B1 and B2. In the present direction of the magnetic field, the difference of the hyperfine fields of the inner sites in the same layers is small, and thus, the signals from the inner sites of A1 and A2 (B1 and B2) are not separable. Note that, unfortunately, the spectra of the outer sites are out of the measured range. The difference between the experimentally obtained [Fig. 2(a)] and simulated [Fig. 2(c)] spectra may come from a slight difference in the directions of the magnetic field and/or the ordered moments between the actual experiment and the simulation. In any case, when an applied magnetic field is nearly parallel to the *b* axis, the ^{13}C-NMR spectra at low temperatures show peaks with positive frequency shifts, though the shifts may be somewhat different among the A1, A2, B1, and B2 sites.

The spectra of 150h-κCl at low temperatures [Fig. 2(b)] do not show clear peaks but show large anomalous broadening, unlike those of 0h-κCl below T_N. With temperature decreased, spectral broadening is developed below around 20 K. This broadening demonstrates a spin-frozen state, which was proposed by the previous ^{1}H-NMR work [18]. Note that broadening is significant on the positive-frequency side, whereas it is not so significant on the negative-frequency side, and broadening spreads to positive frequencies. This indicates that the frozen state is not a conventional SG state, where the local frozen moments are oriented in completely random directions and thus the NMR spectrum spreads equally on the positive- and negative-frequency sides. Because main broadening is on the positive-frequency side, which is similar to the behavior of the shifts due to the AFM moment of 0h-κCl as described above, we infer that the frozen state of 150h-κCl has AFM moments similar to those of 0h-κCl, but the magnitudes of the moments are reduced and distributed continuously. Comparing the tail-edge frequency of the observed spectra at 3.24 K ($\sim$800 kHz) with the simulated spectra using various magnitudes of the AFM moments, we estimate that the maximum value of the moments of 150h-κCl is $\sim$0.23μ_B/dimer [Fig. 2(d)].

As described above, the spectral broadening observed in 150h-κCl is not symmetric but is mainly on the positive-frequency side. We mention lastly the slight broadening to the negative-frequency side, although it only has a minor contribution to the whole intensity. When AFM moments are completely the same as the pristine AFM moments of 0h-κCl, which is almost directed toward the *c* axis, they never produce shifts and/or broadening to negative frequencies in the ^{13}C-NMR spectra. Thus, we consider that a minor fraction of the system (probably around the strong disorder sites) shows spin states completely different from the pristine AFM structure, even in the spin-frozen state.

B. ^{13}C-NMR spin-lattice relaxation rate

The spin-lattice relaxation rate T_1^{-1} of 0h-κCl and 150h-κCl given by the stretched-exponential analysis is shown in Fig. 3. The spin-lattice relaxation rate T_1^{-1} measures the fluctuations on the ^{13}C nuclei on a megahertz time scale. Above $\sim$70 K, T_1^{-1} of 150h-κCl was almost the same as that of 0h-κCl. Note that ^{1}H T_1^{-1} is significantly enhanced by x-ray irradiation even in this temperature region in contrast to the ^{13}C T_1^{-1} behavior. In the previous ^{1}H-NMR work [18], the authors considered that the hyperfine coupling constants of the ^{1}H nuclei are increased by x-ray irradiation because the irradiation causes no meaningful change in the static magnetic susceptibility [25] but disturbs the anions located near the ^{1}H sites [22,27–29]. Our finding supports this consideration by Urai *et al.* and indicates that the hyperfine couplings of the ^{13}C sites, which are far away from the anion layer, are almost unaffected by x-ray irradiation, and those of the ^{1}H sites, which are close to the anion layer, are strongly affected by irradiation. The invariance of the hyperfine couplings of the ^{13}C sites ensures the validity of the previous discussion on the frozen state based on the ^{13}C-NMR spectral data.

Below $\sim$70 K, the behavior of T_1^{-1} of 150h-κCl is different from that of 0h-κCl. This difference suggests that x-ray irradi-
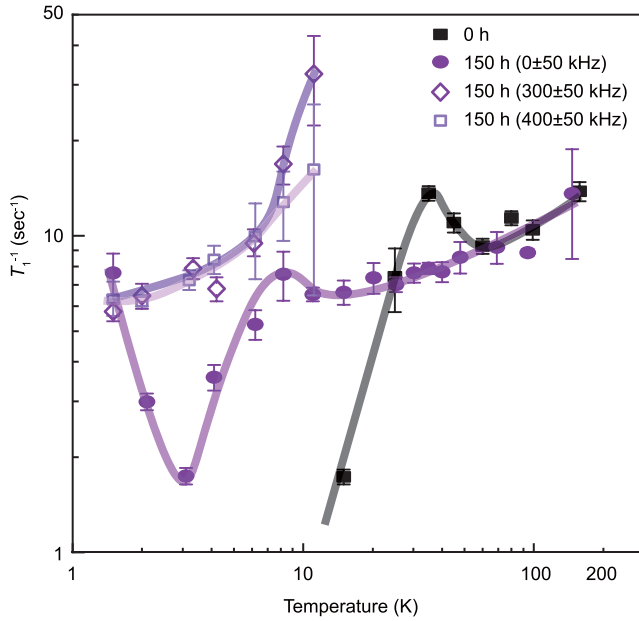
FIG. 3. Temperature dependence of ^{13}C-NMR spin-lattice relaxation rate T_1^{-1} of 0h-κCl (black squares) and 150h-κCl (purple symbols). The data for 150h-κCl at low temperatures are analyzed in the three different frequency ranges, 0 ± 50 kHz (solid dark purple circles), 300 ± 50 kHz (open purple diamonds), and 400 ± 50 kHz (open light purple squares). The data of 0h-κCl are from the previous study [21]. The lines are guides for the eye.

FIG. 4. Temperature dependence of ^{13}C-NMR spin-spin relaxation rate T_2^{-1} of 0h-κCl (black squares) and 150h-κCl (purple symbols). The data for 150h-κCl at low temperatures are analyzed in three different frequency ranges, namely, 0 ± 50 kHz (solid dark purple circles), 300 ± 50 kHz (open purple diamonds), and 400 ± 50 kHz (open light purple squares). The data of 0h-κCl are from the previous study [21].

ation causes a striking change in the electronic state, as is also demonstrated by the spectral results explained in the previous section. As reported in the literature, T_1^{-1} of 0h-κCl shows a peak associated with a slowing down under magnetic field around T_N [34,35]. By contrast, T_1^{-1} of 150h-κCl does not show any peaks at $T = 20$–70 K but decreases continuously from high temperatures. Below 15 K, because of the broadened spectra, we obtained T_1^{-1} in the three different frequency ranges. In the ranges 300 ± 50 and 400 ± 50 kHz, T_1^{-1} shows large values around 15 K and declines below 15 K. The T_1^{-1} data in the range 0 ± 50 kHz shows a small peak around 8 K. These results imply spin freezing. The reason for the large error bar for T_1^{-1} 150h-κCl (400 ± 50 kHz) at $T \sim 10$ K is caused by a strong deviation from the single exponential relaxation, probably due to the Griffith phase nature [38,39], which is explained later. These spin-lattice relaxation rates in the three different frequency ranges do not completely vanish even in the low-temperature limit, in contrast to the data for 0h-κCl. This will be discussed later along with the results of T_2^{-1}.

The spin-lattice relaxation rates in the 0 ± 50 kHz range show a steep upturn below 3 K. A similar upturn at low temperatures was also observed in the previous ^{1}H-NMR work and our ^{1}H-NMR result. In the previous work [18], Urai *et al.* claimed that the upturn is caused by the existence of residual paramagnetic-like spins, which they called "orphan" spins. The present ^{13}C T_1^{-1} result shows that the upturn is observed not in the high-frequency ranges, where the NMR signals are affected by the frozen moments, but only in the range 0 ± 50 kHz, where the paramagnetic-like region contributes
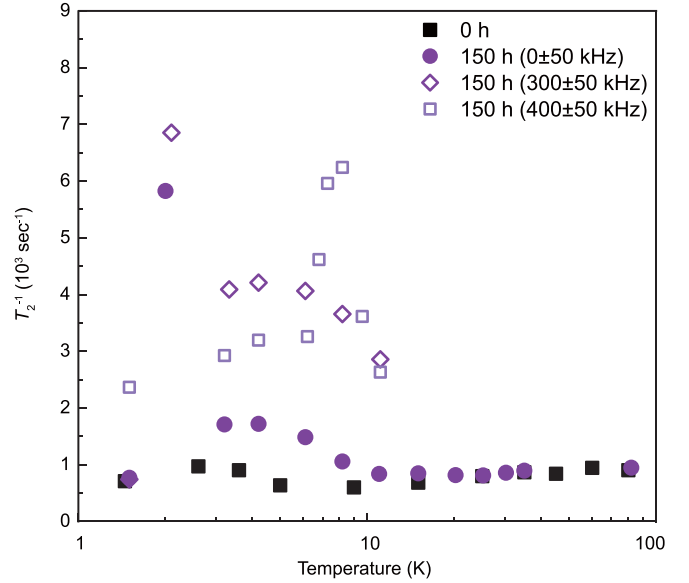
to the NMR signal if it exists. Thus, our result supports the "orphan" spin scenario suggested by Urai *et al.* [21].

C. ^{13}C-NMR spin-spin relaxation rate

Figure 4 shows the temperature dependence of the spin-spin relaxation rate T_2^{-1} of 0h-κCl and 150h-κCl, which was obtained by the analysis explained in the experimental section [40]. The spin-spin relaxation rate in κCl is expressed as $T_2^{-1} = T_{2L}^{-1} + T_{2G}^{-1}$, where T_{2L}^{-1} and T_{2G}^{-1} measure the fluctuations on the ^{13}C nuclei on a kilohertz time scale (the temperature-dependent component) and the nuclear-nuclear magnetic-dipole coupling (the temperature-independent component), respectively. Taking the crystal structure of κCl into account, we estimated T_{2G}^{-1} to be approximately 1000 s^{-1} [21]. We note that ^{1}H-NMR T_{2G}^{-1} for κCl is much larger than ^{1}H-NMR T_{2L}^{-1}, and thus, ^{1}H-NMR T_{2L}^{-1}, or information on kilohertz fluctuations, cannot be obtained in the previous ^{1}H-NMR work [18]. As shown in Fig. 4, T_2^{-1} of ^{13}C-NMR for 0h-κCl shows a temperature-independent value of approximately 1000 s^{-1}, which means that T_2^{-1} of 0h-κCl is dominated by T_{2G}^{-1}, and kilohertz fluctuations of this system are too small to detect. For 150h-κCl, T_2^{-1} also has the same temperature-independent value at high temperatures. By contrast, T_2^{-1} of 150h-κCl shows a significant enhancement from this value below $\sim$15 K, indicating that kilohertz dynamics is strongly developed at low temperatures. Note that we cannot discuss the detailed behavior of this kilohertz dynamics. This is because although a correct value of T_2^{-1} can be obtained only when the entire spectrum is within the measurable frequency range restricted by the $\pi/2$ and π pulse widths, the spectra at low temperatures (below $\sim$15 K) are well beyond

this range as shown in Fig. 2(b). In this case, the obtained values of T_2^{-1}, shown in Fig. 4, are underestimated. Thus, it is impossible to obtain the correct values of T_2^{-1} and to discuss the detailed behavior of the kilohertz dynamics at low temperatures. Anyway, these data mean that the kilohertz fluctuation is developed at low temperatures. Taking into account that T_1^{-1} does not vanish and T_2^{-1} shows an enhancement at low temperatures, we presume that the frozen moments fluctuate very slowly around the stable directions at low temperatures.

D. Possibility of the Griffiths phase

We consider that the slow dynamics observed in the frozen state of 150h-κCl is due to the "Griffiths physics" [38,39]. In general, introduced randomness spreads a critical point into a widely spread critical region, which shows slow fluctuations of the order parameter reminiscent of critical slowing down in the original pure system. Here, we note that the Mott transition system κCl has two different critical behaviors in its pressure-temperature phase diagram: one is the critical behaviors due to the AFM transition realized in the spin sector [23,35], and the other is due to the Mott transition realized in the charge sector [41–43]. From the simple standpoint, these two criticalities cause different Griffiths physics, that is, conventional magnetic Griffiths physics and electronic Griffiths physics.

Basically, it is natural to think that the slow dynamics observed in the present system, 150h-κCl, is in the spin sector and is thus related to the magnetic Griffiths physics because the system shows spin freezing. It is interesting that a further x-ray-irradiated system (500h-κCl), which no longer shows any spin ordering but instead is situated just on the Mott boundary, also shows electronic slow dynamics [21]. It is natural to think that this slow dynamics of 500h-κCl is, in turn, realized in the charge sector because the system does not show spin freezing but is on the Mott boundary. However, it is not clear whether such a simple idea of assuming so-called spin-charge separation is valid, and these spin and charge Griffiths physics may not be separable but may be intertwined. Note that such a simple idea of assuming so-called spin-charge separation is valid only when the first-order Mott transition is well defined. When the first-order Mott transition is well defined, the Mott insulator at temperatures much lower than the critical end-point temperature only has spin excitations. However, in the present x-ray-irradiated system, the Mott transition may be smeared and not well defined [43,44]. In this case, it is not trivial whether the idea of assuming spin-charge separation is

valid, and these spin and charge Griffiths behaviors may not be separable but may be intertwined. Although 150h-κCl is basically at the Mott-insulator side [43,44], the slow dynamics observed in 150h-κCl might be dominated not only by the spin degree of freedom but also by the charge degrees of freedom to some degree.

In the disordered Mott transition systems 500h-κCl [21] and EtMe$_3$Sb[Pd(dmit)$_2$]$_2$ [45], which are situated on the Mott boundary and do not show any magnetic freezing, the electronic Griffith dynamics has been observed in the QSL-like state. By contrast, because 150h-κCl is basically at the Mott-insulating side, it shows the SG-like state and slow dynamics probably related to magnetic freezing. It is difficult to compare EtMe$_3$Sb[Pd(dmit)$_2$]$_2$ with 150h-κCl directly, but it is meaningful to investigate how the dynamics of 150h-κCl is changed into that of 500h-κCl by increasing randomness. We believe that further work to study slow dynamics in disordered Mott transition systems is needed, and this will open a new avenue for understanding Mott-related physics such as the disorder-induced QSL state.

IV. CONCLUSION

We have investigated the unconventional SG-like state realized in 150-h x-ray-irradiated κCl using ^{13}C-NMR measurements. We have shown that in the SG-like state, the spin moments in the major fraction inherit the pristine AFM structure of nonirradiated κCl but their magnitudes are reduced and distributed continuously, whereas there are also minor spins that differ from the pristine AFM structure.

These frozen moments in the SG-like state fluctuate very slowly around the stable directions even at low temperatures. This feature suggests that the weak randomness effect on the AFM state of κCl causes the magnetic Griffiths nature. The relation between the present magnetic Griffiths physics and electronic Griffiths physics observed in the further x-ray-irradiated system will be the subject of future study.

ACKNOWLEDGMENTS

[1] J. Villain, Z. Phys. B **33**, 31 (1979).

[2] R. N. Bhatt and P. A. Lee, Phys. Rev. Lett. **48**, 344 (1982).

[3] A. P. Ramirez, Annu. Rev. Mater. Sci. **24**, 453 (1994).

[4] Y.-C. Lin, R. Mélin, H. Rieger, and F. Iglói, Phys. Rev. B **68**, 024424 (2003).

[5] S. Dey, E. C. Andrade, and M. Vojta, Phys. Rev. B **101**, 020411(R) (2020).

[6] L. J. de Jongh, in *Magnetic Phase Transitions*, edited by M. Ausloos and R. J. Elliott (Springer, New York, 1983), p. 172.

[7] N. Tristan, V. Zestrea, G. Behr, R. Klingeler, B. Büchner, H.-A. Krug von Nidda, A. Loidl, and V. Tsurkan, Phys. Rev. B **77**, 094412 (2008).

[8] K. Hanashima, Y. Kodama, D. Akahoshi, C. Kanadani, and Toshiaki Saito, J. Phys. Soc. Jpn. **82**, 024702 (2013).

[9] D. C. Johnston, J. P. Stokes, D. P. Goshorn, and J. T. Lewandowski, Phys. Rev. B **36**, 4007 (1987).

[10] S-W. Cheong, A. S. Cooper, L. W. Rupp, Jr., B. Batlogg, J. D. Thompson, and Z. Fisk, Phys. Rev. B **44**, 9739 (1991).

[11] M. Corti, A. Rigamonti, F. Tabak, P. Carretta, F. Licci, and L. Raffo, Phys. Rev. B **52**, 4226 (1995).

[12] S.-H. Lee, H. Kikuchi, Y. Qiu, B. Lake, Q. Huang, K. Habicht, and K. Kiefer, Nat. Mater. **6**, 853 (2007).

[13] M. R. Norman, Rev. Mod. Phys. **88**, 041002 (2016).

[14] P. Mendels and F. Bert, C. R. Phys. **17**, 455 (2016).

[15] K. Watanabe, H. Kawamura, H. Nakano, and T. Sakai, J. Phys. Soc. Jpn. **83**, 034714 (2014).

[16] T. Shimokawa, K. Watanabe, and H. Kawamura, Phys. Rev. B **92**, 134407 (2015).

[17] H. Kawamura and K. Uematsu, J. Phys.: Condens. Matter **31**, 504003 (2019).

[18] M. Urai, K. Miyagawa, T. Sasaki, H. Taniguchi, and K. Kanoda, Phys. Rev. Lett. **124**, 117204 (2020).

[19] E. C. Andrade, E. Miranda, and V. Dobrosavljević, Phys. Rev. Lett. **102**, 206403 (2009).

[20] I. F. Mello, L. Squillante, G. O. Gomes, A. C. Seridonio, and M. de Souza, J. Appl. Phys. **128**, 225102 (2020).

[21] R. Yamamoto, T. Furukawa, K. Miyagawa, T. Sasaki, K. Kanoda, and T. Itou, Phys. Rev. Lett. **124**, 046404 (2020).

[22] T. Sasaki, Crystals **2**, 374 (2012).

[23] K. Miyagawa, A. Kawamoto, Y. Nakazawa, and K. Kanoda, Phys. Rev. Lett. **75**, 1174 (1995).

[24] M. Ito, T. Uehara, H. Taniguchi, K. Satoh, Y. Ishii, and I. Watanabe, J. Phys. Soc. Jpn. **84**, 053703 (2015).

[25] T. Furukawa, K. Miyagawa, T. Itou, M. Ito, H. Taniguchi, M. Saito, S. Iguchi, T. Sasaki, and K. Kanoda, Phys. Rev. Lett. **115**, 077001 (2015).

[26] E. Scriven and B. J. Powell, Phys. Rev. B **80**, 205107 (2009).

[27] N. Yoneyama, T. Sasaki, N. Kobayashi, K. Furukawa, and T. Nakamura, Physica B (Amsterdam) **405**, S244 (2010).

[28] L. Kang, K. Akagi, K. Hayashi, and T. Sasaki, Phys. Rev. B **95**, 214106 (2017).

[29] A. K. R. Ang, R. Marumi, A. Sato-Tomita, K. Kimura, N. Happo, K. Akagi, T. Sasaki, and K. Hayashi, Phys. Rev. B **103**, 214106 (2021).

[30] D. F. Smith, S. M. De Soto, C. P. Slichter, J. A. Schlueter, A. M. Kini, and R. G. Daugherty, Phys. Rev. B **68**, 024512 (2003).

[31] B. L. Henke, E. M. Gullikson, and J. C. Davis, At. Data Nucl. Data Tables **54**, 181 (1993).

[32] N. Yoneyama, T. Sasaki, N. Kobayashi, Y. Ikemoto, and H. Kimura, Phys. Rev. B **72**, 214519 (2005).

[33] H. Taniguchi, K. Kanoda, and A. Kawamoto, Phys. Rev. B **67**, 014510 (2003).

[34] F. Kagawa, Y. Kurosaki, K. Miyagawa, and K. Kanoda, Phys. Rev. B **78**, 184402 (2008).

[35] A. Kawamoto, K. Miyagawa, Y. Nakazawa, and K. Kanoda, Phys. Rev. B **52**, 15522 (1995).

[36] R. Ishikawa, H. Tsunakawa, K. Oinuma, S. Michimura, H. Taniguchi, K. Satoh, Y. Ishii, and H. Okamoto, J. Phys. Soc. Jpn. **87**, 064701 (2018)

[37] S. M. De Soto, C. P. Slichter, A. M. Kini, H. H. Wang, U. Geiser, and J. M. Williams, Phys. Rev. B **52**, 10364 (1995).

[38] R. B. Griffiths, Phys. Rev. Lett. **23**, 17 (1969).

[39] T. Vojta, AIP Conf. Proc. **1550**, 188 (2013).

[40] In this study, the decay term of the spin-echo intensity curve was fitted using Gaussian decay, $\exp(-(2\tau/T_2)^2)$, in the whole temperature range. Decay terms of the spin-echo intensity curves become (a) Gaussian decay, $\exp(-(2\tau/T_{2G})^2)$, when magnetic interactions between like nuclei mainly cause the decay and (b) exponential decay, $\exp(-2\tau/T_{2L})$, when fluctuations of the internal magnetic field in the kilohertz frequency range do. In principle, we should therefore take the decay term to be the product of the Gaussian and exponential functions, with two T_2's (T_{2G} and T_{2L}): $\exp(-(2\tau/T_{2G})^2)\exp(-2\tau/T_{2L})$. Nevertheless, we have assumed only the Gaussian decay, thus obtaining T_2^{-1}, which contains information about both T_{2G}^{-1} and T_{2L}^{-1} because this fitting has only one parameter, which can be determined more precisely and which can capture the qualitative properties of T_{2L}^{-1} thanks to the temperature independence of T_{2G}^{-1} in the present system.

[41] F. Kagawa, K. Miyagawa, and K. Kanoda, Nature (London) **436**, 534 (2005).

[42] T. Furukawa, K. Miyagawa, H. Taniguchi, R. Kato, and K. Kanoda, Nat. Phys. **11**, 221 (2015).

[43] M. Urai, T. Furukawa, Y. Seki, K. Miyagawa, T. Sasaki, H. Taniguchi, and K. Kanoda, Phys. Rev. B **99**, 245139 (2019).

[44] E. Gati, U. Tutsuch, A. Naji, M. Garst, S. Köhler, H. Schubert, T. Sasaki, and M. Lang, Crystals **8**, 38 (2018).

[45] T. Itou, E. Watanabe, S. Maegawa, A. Tajima, N. Tajima, K. Kubo, R. Kato, and K. Kanoda, Sci. Adv. **3**, e1601594 (2017).